Anomalous Enhancement of Interphase Transport Rates by Nanoparticles: Effect of Magnetic Iron Oxide on Gas–Liquid Mass Transfer

ARTICLE *in* INDUSTRIAL & ENGINEERING CHEMISTRY RESEARCH · NOVEMBER 2009

Impact Factor: 2.59 · DOI: 10.1021/ie900302z

2 AUTHORS, INCLUDING:

A.K. Suresh

Indian Institute of Technology Bombay

71 PUBLICATIONS **1,197** CITATIONS

SEE PROFILE

Anomalous Enhancement of Interphase Transport Rates by Nanoparticles: Effect of Magnetic Iron Oxide on Gas−Liquid Mass Transfer

Srinivas Komati and Akkihebbal K. Suresh*

Department of Chemical Engineering, Indian Institute of Technology, Mumbai 400076, India

In this paper, we examine the effect of magnetic iron oxide nanoparticles on gas−liquid mass transfer rates. Carbon dioxide and oxygen are the gases absorbed, into a variety of reactive and nonreactive liquids. Experiments have been carried out in a wetted wall column (where the hydrodynamics can be rigorously modeled) and in a capillary tube (with the liquid phase being quiescent). In the case of absorption with reaction, studies have been conducted in several absorption regimes, representing different levels of transport limitations. The experiments convincingly demonstrate that the liquid phase mass transfer coefficients are significantly enhanced in the presence of nanoparticles in the region of concentration gradients, the extent of enhancement depending on the volume fraction of solid particles in the fluid, and on the particle size scaled with respect to the depth of penetration of the diffusing solute. A modified Sherwood number has been identified, based on the traditional theories of interphase mass transfer, as the dominant parameter which determines the magnitude of the mass transfer intensification effect at a given particle holdup, and a correlation has been derived for the enhancement, which explains not only the data obtained in this work, but also data from the literature. The enhancement effect, having been observed in the presence and absence of reaction and flow, points to the fundamental molecular-level transport processes being influenced by the nanoparticles, but the exact mechanisms remain to be established.

1. Introduction

In recent years, there has been a lot of interest on the unique properties of matter on the nanometer length scale and on harnessing these properties in engineering applications. Many new applications of nanomaterials continue to be found although the physical basis that underlies these applications is not always well-understood. The chemical process industry, being fundamentally concerned with the rate processes of reaction and transport, is watching keenly the possibilities nanotechnology offers in these areas. In the area of reactions and reaction engineering, the discipline of catalysis is already seeing significant developments due to nanomaterials. As for transport processes, while there are reports of interesting effects of nanoparticles, a consensus, and a broad basis for prediction and design, have so far been elusive. For example, there are reports, ill-understood and sometimes contested, of anomalous increases in thermal conductivities of liquids when nanoparticulate solids are added,[1] the enhancement being dependent on the particle size and volume fraction.[2,3] Likewise, there are reports on the convective heat transfer coefficients being enhanced by the presence of nanoparticles.[4−8] On mass transport, the literature is more limited (and on the whole more confusing), but several claims of significant enhancement in rates do exist. The available theories[9−11] of "fine particle-enhanced mass transfer" do not predict the large enhancements seen. An issue here is that, in the bubbling contactors of practical interest, the transfer areas are not constant but depend in a nontrivial way on the properties of the liquid phase. Thus in the few studies that are available on the effect of nanoparticles on mass transfer, it is often difficult to say whether it is the mass transfer coefficient or interfacial area that is influenced. The present work is motivated by this confusion that exists in the literature on the effect of nanoparticles on interphase mass transfer. Systematic studies using model apparatus and model reactions, built upon the classical theories of mass transfer, have been carried out to examine the potential of nanofluids to impact mass transfer rates, and to explore the important parameters on which the effect (if any) depends.

Most of the literature on the effect of nanoparticles on mass transfer has employed ferrofluids, which are stabilized suspensions of single-domain, super paramagnetic iron oxide nanoparticles. Suresh and Bhalerao[12] tested out a strategy of adding a ferrofluid to the liquid phase of a gas−liquid system and manipulating the particles using an oscillating magnetic field external to the apparatus. The expectation was that the particles, because of their tendency to follow the field, would bring about mixing in the near interface region, and hence, an enhancement in absorption rates. In their studies in a wetted wall column and a bubble column, they observed a 40−50% enhancement with this strategy. The authors concluded that the full potential of the strategy would be much higher than their results indicated, but could not be realized in their work due to two reasons: (1) the surfactant coating of the particles was destabilized in their high ionic strength solutions, with the particles quickly growing to micrometer dimensions, and (2) much of the work was carried out in the instantaneous reaction regime with the solute concentration gradients being confined to a thin layer next to the interface. These authors did not observe much of an effect of the particles themselves in the absence of the field. Subsequent work by Olle et al.[13] and Komati and Suresh[14] shows that nanoparticles by themselves can enhance mass transfer rates. The work of Komati and Suresh,[14] in particular, employed the wetted wall column, in which constancy of interfacial area can be ascertained by visual observation. Further, the conditions of their experimentation allowed for both mass transfer coefficient and interfacial area to be determined from the data under some assumptions. From their results, these authors argued that the observed enhancement in mass transfer rates is attributable solely to that in the mass transfer coefficients. A comparison of these results with those of Komati et al.[15] in

* Corresponding author. Tel.: +91-22-25767240. Fax: +91-22-25726895. E-mail: aksuresh@iitb.ac.in.

10.1021/ie900302z
Published on Web 11/19/2009

a bubble column led the authors to speculate that the magnitude of enhancement (for a given particle size) depends on the thickness of the region in which concentration gradients of the diffusing solute lie. In other work, Krishnamurthy et al.[16] studied the diffusive spread of a dye spot and claimed that the diffusion of a dye is over 10-fold faster in a nanofluid than in water. Their studies employed 20 nm Al_2O_3 nanoparticles, at a volume fraction of nanoparticles of 0.5%. While the dye spot expands symmetrically by diffusion in the absence of particles, this is no longer the case when particles are present, and quantitative interpretation of their results is rendered difficult for that reason. Kim et al.[17] studied the effect of nanofluids of Cu, CuO, and Al_2O_3 of 50 nm on the absorption rate of NH_3 in water using a bubble absorber and concluded that the absorption rate increased with increasing concentration of nanoparticles.

While the literature is thus strongly indicative of the potential of nanoparticles (especially those of magnetic iron oxide) to enhance mass transfer rates, the fact is not established beyond a doubt, as some of the evidence is conflicting. There are also uncertainties as to the magnitude of the effect (where claimed) because of an unclear separation between the mass transfer coefficient and the interfacial area. Further, the data do not clearly point to the important parameters on which the enhancement depends and, hence, do not afford any possibility of generalization to other systems. The present work is motivated by these deficiencies in the extant literature. We have studied gas−liquid mass transfer rates in the presence and absence of different ferrofluids, in different gas−liquid systems and different contactors, and in the presence and absence of chemical reactions, in order to arrive at some generalizations on the effect of nanoparticles on interface mass transfer. To this end, we have synthesized a range of ferrofluids with the required stability in the solutions of interest. Our results show that the enhancement in mass transfer coefficients depends on a scaling parameter, using which much of the conflicting results in the literature can be rationalized.

2. Experimental Methods

2.1. Ferrofluid Synthesis and Characterization. In choosing the ferrofluids to work with, the need to ensure sufficient stability in our solutions of interest and the ability to use a range of particle sizes have been the guiding criteria in the present work. Three types of aqueous ferrofluids, with differences in the particle size and method of stabilization, have been used. The first, synthesized in our laboratories, used a liquid phase coprecipitation technique, which involved neutralizing solutions of ferrous and ferric chlorides with ammonia,[18] and stabilization by tetramethylammonium hydroxide (TMAOH) surfactant. The method has been discussed in detail elsewhere,[15,18] and details of characterization have been presented in our earlier work.[15] The second ferrofluid, procured from Bhavnagar University, was essentially similar, but used lauric acid as the surfactant for stabilization. The third was prepared, as described by Moeser et al.[19] by chemical coprecipitation in a graft copolymer solution. The ferrofluid was stabilized in this case by the polymer attached to the surface. Graft copolymers were prepared by reacting poly(acrylic acid) (PAA) with amino terminated polyethylene oxide (PEO).

The ferrofluids were characterized with respect to their particle size distribution, iron oxide phases, surface area, magnetization, and size stability in the solutions of interest. The size distribution was primarily determined by dynamic light scattering (DLS), using a Brookhaven Zeta Plus instrument with BI-MAS attachment. Size and shape were also checked by taking TEM images using a Philips CM200 TEM with 200 kV accelerating voltage (see Komati et al.[15] for details). Further confirmation of size was obtained from X-ray diffraction (XRD) patterns through the use of the Debye−Scherrer equation. Size stability of the ferrofluids in the liquids of interest, was determined by measuring particle size distributions of the ferrofluids in the solutions of interest, as a function of time by DLS as already described.

Phase identification was carried out using XRD (Philips X′Pert PRO diffractometer) and Raman spectroscopy (on a Lab RAM HR 800 Instrument). The methods were standard and have been described in our earlier work.[15] In order to examine whether the nanoparticles are influenced in any way by the reactions being studied, the phase characterization of the magnetic nanoparticles in the ferrofluid was performed before and after chemical absorption of carbon dioxide into amine solutions using XRD, as described earlier. These data also provide a check on the particle sizes before and after the reaction.

The specific surface area of the Fe_3O_4 nanoparticles in the ferrofluids was measured by the Brunauer−Emmett−Teller (BET) method, using an America Micromeritics ASAP-2020 analyzer. Nitrogen adsorption−desorption isotherms at 77.35 K were used in this measurement.

The magnetization of the Fe_3O_4 particles was measured by VSM (variable sample magnetometry) at 298 K and ± 20 000 G applied magnetic field (Oxford VSM, maglab). Sample preparation for VSM was similar to that described above for XRD.

2.2. Mass Transfer Studies−Apparatus Used. Two model gas−liquid contactors have been used in the mass transfer studies described in this work, and data from a third, a bubble column described in an earlier work,[15] have also been used for comparison. The first was a wetted wall column (WWC), constructed from a stainless steel tube of outside diameter 1.3 cm and a maximum height of 17.3 cm. The tube is placed inside a glass enclosure that permits a dead-end operation with respect to the gas. The gas space is connected to a gas balloon through a soap bubble flow meter, which directly measures the rate of absorption of the gas, from which the value of the mass transfer coefficient can be calculated. The WWC design was as described in the work of Roberts and Danckwerts[20] except that a provision was made to dose the ferrofluid using a syringe pump where the liquid enters the column. The design and operating procedures have been described in detail in our previous work.[14] Before using the WWC in the mass transfer studies of interest, the column design and operation were checked using CO_2 absorption into carbonate−bicarbonate buffers. The WWC provided for absorption studies in a simple hydrodynamic situation amenable to modeling, so that the mass transfer coefficients for the base case of absorption into homogeneous liquid phases (without nanoparticles) can be predicted completely from first principles and checked from experiments.

The second apparatus consisted essentially of a capillary connected to a gas balloon, and a simple experiment was devised using this apparatus to study unsteady state gas absorption into a stagnant liquid. The experiment consisted in following the size of a gas slug, in contact with a stagnant liquid column, with time as the liquid absorbed the gas. A schematic diagram of the experimental setup is shown in Figure 1. The capillary, of 4 mm internal diameter, was initially filled completely with the liquid of interest, and one end of the capillary connected to the CO_2 balloon (that contained carbon dioxide saturated with water vapor at the temperature of interest). The liquid column

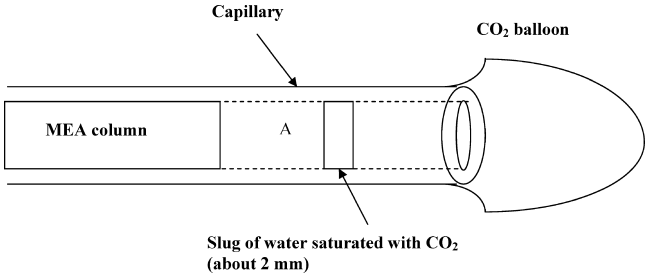

Figure 1. Schematic diagram of the capillary apparatus used in unsteady state absorption studies of carbon dioxide into quiescent liquid columns.

was withdrawn a little to the left (by gravity or suction) in order to suck in some of the gas. The gas balloon was disconnected, a small slug of water saturated with CO_2 was inserted, and the capillary was reconnected to the CO_2 balloon, thereby trapping a gas slug (compartment A in Figure 1). The liquid column was moved a little more toward left, and the position of the water slug was marked. The absorption process was then monitored by following the position of the water slug with respect to time.

In our earlier studies,[15] we have reported results from studies in a bubble column, as a representative of the bubble−swarm contactors common in industrial practice. The column was 30 mm in internal diameter, 450 mm in height, and used a sintered glass plate as a sparger. Mass transfer rate measurements, in absorption-with-chemical reaction, were carried out by causing the gas to bubble at a constant flow rate for a known length of time, and analyzing the liquid phase for the conversion achieved. In the sequel, these results (as well as some other data from the literature) will be compared with the results from the model apparatuses described above.

This choice of apparatuses and systems (to be described below) enabled studies under different absorption regimes and hydrodynamic conditions. In the reaction experiments with ferrofluids, the reagents (amine solutions) were prepared such that the required concentrations of the liquid phase reactant were achieved after the addition of the ferrofluid. This was also ascertained by determination of the concentration in the ferrofluid-added solutions by volumetric methods as described in Komati and Suresh.[14] All experiments were conducted at room temperature (25 °C) and at least in duplicate. Since the absorption in WWC and capillary can be rigorously modeled, the base case of absorption in the absence of ferrofluid always provided a check on the experimental protocol.

2.3. Mass Transfer Studies−Gas−Liquid Systems and Absorption Regimes. Studies were carried out with several gas−liquid systems, with and without reaction. The theory of mass transfer with chemical reaction[21] describes several absorption "regimes" depending on the relative rates of diffusion and reaction, which differ in how the absorption rate depends on the system parameters. Thus, when absorption of a gaseous solute A is accompanied by a liquid phase reaction

$$\mathrm{A(g)} + z\mathrm{B(l)} \rightarrow \text{product}$$

which is of order m in the gaseous solute A, order n in the liquid phase reactant B, and is fast enough to influence the mass transfer rates, the absorption flux R_A (mol/(m^2 s)) is, in general, increased by an "enhancement factor" E and is given by

$$R_A = k_L C_A^* E \tag{1}$$

The magnitude of E depends on the absorption regime and has been addressed using different theories of mass transfer (film, penetration, and surface renewal). For the most part, the predictions of the theories are close, and the value of E is determined by the magnitudes of two parameters: the Hatta number

$$Ha = \frac{\sqrt{\frac{2}{m+1} D_A k_{mn} (C_A^*)^{m-1} C_{B0}^n}}{k_L} \tag{2}$$

and the parameter

$$q = \frac{D_B C_{B0}}{z D_A C_A^*} \tag{3}$$

D_A andD_B are the diffusivities of A and B in the liquid phase, k_{mn}, the reaction rate constant, C_A^*, the solubility of the gas in the liquid, and C_{B0}, the concentration of B in the liquid. The term $k_L$is the liquid phase mass transfer coefficient in the absence of any chemical reaction. The influence of the reaction on mass transfer would be felt whenever $Ha \geq 1$, and by arranging the values of the above two parameters appropriately, different regimes can be engineered and different quantities which influence the absorption rates can be determined from the measured absorption rates. This forms the basis of the so-called "chemical methods" for determining various mass transfer parameters for a given contactor and has been used in the present work. Using a range of gas−liquid systems, absorption with and without chemical reaction, and in the latter case, in several absorption regimes, has been studied. These systems and the theory used in interpreting the data are briefly described in the following paragraphs.

Physical Absorption. In this case, the liquid phase contains no reactant, and absorption occurs by a process of dissolution and diffusion. These studies were carried out in the capillary tube. Carbon dioxide was the gas employed. Referring to Figure 1 and assuming the gas slug A to be right cylindrical to a good approximation, if the length changes from L_1 to L_2 during the period $0-t$, an *average* mass transfer coefficient k_L over this period can be calculated from

$$[C_G(L_1 - L_2)] = k_L C_A^* t \tag{4}$$

where C_G is the concentration of the gas in the gas chamber A (calculated from ideal gas law and accounting for the partial pressure of water). The Fickian nature or otherwise of the diffusion process involved, may be examined from the time variation of the slug length, as follows. The length L of the gas slug A at any time t, as it shrinks due to uptake of the gas by the liquid column during the experiment, is related to the *instantaneous* absorption rate per unit area, R_A, as

$$C_G \frac{dL}{dt} = R_{Ai} \tag{5}$$

R_{Ai} is to be obtained by the solution of the unsteady state diffusion equation of the gaseous solute into an infinite column of liquid. For Fickian diffusion in a nonreactive liquid, the theory[21] gives, ignoring the curvature of the liquid meniscus

$$R_{Ai} = C_A^* \sqrt{\frac{D_A}{\pi t}} = k_{Li} C_A^* \tag{6}$$

where k_{Li} is an *instantaneous* mass transfer coefficient. Substituting into 5 and integrating from time 0 to time t, we get

$$L_1 - L_2 = \frac{k_L C_A^* t}{C_G} = \left[2\sqrt{\frac{D_A}{\pi}\frac{C_A^*}{C_G}}\right]\sqrt{t} \tag{7}$$

showing that the length of the slug (and the time-average mass transfer coefficient) would show a square-root dependence on time for Fickian diffusion.

Absorption in the Slow-to-Fast Transition Regime. If the conditions are such that $Ha \ll q$ and $1 < Ha < 3$, the absorption is said to occur in the slow-to-fast transition regime, and using the expression for E provided by Danckwerts' surface renewal theory,[21] we get for the rate of absorption in this regime:

$$R_A a = aC_A^* \sqrt{\frac{2}{m+1} D_A k_{mn} (C_A^*)^{m-1} C_{B0}^n + {k_L}^2} \qquad (8)$$

where "a" is the interfacial area available for transport. Thus, experimental measurements of absorption rate at different values of the rate constant can be plotted in a manner that yields the values of k_L and a separately, if other quantities in the expression are known.

In the present work, the WWC has been used for studies in this regime, in conjunction with two systems: CO_2−methyldiethanolamine (MDEA) and O_2−sodium dithionite. Details for the first system have been given in the work of Komati and Suresh.[14] This reaction follows a pseudo-first-order reaction in which the rate constant k_{ov} can be varied via MDEA and OH^- concentrations. The reaction of oxygen with sodium dithionite follows[22]

$$Na_2S_2O_4 + H_2O + O_2 \rightarrow NaHSO_3 + NaHSO_4$$

For dithionite concentrations below 80 mol/m^3, the reaction is first order in dithionite and zero order in oxygen. The value of the rate constant (first order) k_1 has been assumed to be 8 s^{-1} as reported by Jhaveri and Sharma.[22]

While the predictions of Danckwerts' surface renewal theory are close to those of the penetration theory under most conditions,[23] the hydrodynamics of the WWC are such that the latter theory applies better. The equation that the penetration theory gives for the enhancement factor is

$$E = \frac{\pi}{4Ha}\left[\left(\frac{4Ha^2}{\pi} + \frac{1}{2}\right)\mathrm{erf}\left(\frac{2Ha}{\sqrt{\pi}}\right) + \frac{2Ha}{\pi} e^{-4Ha^2/\pi}\right] \qquad (9)$$

Therefore, the estimates of k_L obtained as described above were used as initial guesses and refined values calculated from this expression, using appropriate nonlinear regression tools from MATLAB.

Absorption in the Fast Reaction Regime. The defining conditions for this regime are $3 < Ha \ll q$ The absorption rate in this regime is independent of the physical mass transfer coefficient, and, hence, the hydrodynamics, since E in eq 1 is given by all the major theories[21,23] as $E = Ha$. In our WWC, the CO_2−MDEA system can be operated in the fast reaction regime for concentrations of MDEA (C_{B0}) of 4000 mol/m^3. As the rate expressions show, the quantity $(D_A k_1)^{1/2}$ (where k_1 is the overall first-order rate constant) can be calculated from measured absorption rates in this regime.

Absorption in the Instantaneous Reaction Regime. If $Ha \gg q$, the absorption occurs in the "intantaneous reaction regime" in which both A and B diffuse to a reaction plane and react there. The penetration distance of the dissolving solute is thus much smaller in this regime as compared to the other regimes for a given hydrodynamic condition. These experiments were conducted in the capillary apparatus (where absorption rate changes with time) and in the WWC (in which an average rate of absorption over the residence time of the liquid in the column is measured). For a given value of q, the enhancement E obtained in this regime (designated as E_∞) is the highest possible, and is given by the penetration theory as

$$E_\infty = \frac{1}{\mathrm{erf}\left(\frac{\beta}{\sqrt{D_A}}\right)} \qquad (10)$$

where β is a parameter that determines the (time-dependent) location of the reaction plane as given by $2\beta\sqrt{t}$ (measured from the interface). β is given by

$$e^{\beta^2/D_B}\,\mathrm{erfc}(\beta/\sqrt{D_B}) = \frac{C_{B0}}{zC_A^*}\sqrt{\frac{D_B}{D_A}} e^{\beta^2/D_A}\,\mathrm{erfc}(\beta/\sqrt{D_A}) \qquad (11)$$

For large enhancements, the following approximation[21] is convenient for calculating E_∞:

$$E_\infty = \sqrt{\frac{D_A}{D_B}} + \frac{C_{B0}}{zC_A^*}\sqrt{\frac{D_B}{D_A}} \qquad (12)$$

Using E_∞ in eq 1, substituting into eq 5 for the length of the gas slug in the capillary, we get

$$L_1 - L_2 = \frac{k_L C_A^* t E_\infty}{C_G} = \left[2\sqrt{\frac{D_A}{\pi}}\frac{C_A^*}{C_G}\right] E_\infty \sqrt{t} \qquad (13)$$

showing once again the square root dependence of slug length with time, for Fickian diffusion with a constant diffusivity.

The results in the WWC can be interpreted using the same expressions (eqs 1 and 10) for the enhancement factor and allow an estimation of the mass transfer coefficient. While the concentrations used ensured $Ha \gg q$ (as required for the instantaneous regime) in the absence of ferrofluids, the mass transfer enhancements caused in the presence of the latter sometimes lowered the values of Ha for cases with ferrofluids. While the Hatta number still remained larger than q, the difference between the two was lowered in these cases. To ensure consistency in the calculations, the values of (chemical) enhancement factors in such cases were corrected by using the expressions available[21] for transition from fast to instantaneous regime. It was found that in general, the values of k_L thus obtained were not much different from those obtained assuming instantaneous regime.

The gas−liquid system used in the instantaneous regime studies in the present work was CO_2−monoethanolamine (MEA). The reaction is

$$CO_2 + 2HOC_2H_4NH_2 \rightleftharpoons HOC_2H_4NH_3^+ + HOC_2H_4NHCOO^-$$

The kinetics of the reaction were taken from the work of Laddha and Danckwerts[24] and Hikita et al.[25] and used to calculate the concentrations to be used to ensure instantaneous reaction regime.

2.4. Other Properties in the Presence and Absence of Ferrofluids. In order to examine the effect of the added ferrofluid on solubility, the solubilities of CO_2 in water, ferrofluids, and methyldiethanolamine solutions were measured both in the presence and absence of the ferrofluid. Due to the chemical reaction between CO_2 and amines, free gas solubility cannot be measured directly, so N_2O analogy was used to measure CO_2 solubility into amine solutions as described by Al-Ghawas et al.[26] and Haimour.[27] The N_2O analogy for the solubility of CO_2 into amine solutions is as follows.

$$H_{CO_2} = H_{N_2O}\left(\frac{H_{CO_2}}{H_{H_2O}}\right)_{water} \qquad (14)$$

Where H_{CO_2} and H_{N_2O} are the Henry's law coefficients for a CO_2−MDEA system and an N_2O−MDEA system, respectively. The apparatus and experimental protocol for the determination of solubility were identical to those described by Al-Ghawas et al.[26] and Haimour.[27]

In order to explain some features of the intensification effect of nanofluids when interpreted in terms of diffusivity enhance-

Table 1. Summary of Characterization Studies on the Ferrofluids Used in This Work

property		polymer-coated ferrofluid	lauric acid-coated ferrofluid	TMAOH-coated ferrofluid
average Size, nm	DLS	13.2	10	21.1
	BET	6.5	7.2	14.1
	TEM	7	8	15
	XRD	7.1	7.8	15.2
particle volume fraction, mL of solid magnetite/ mL of ferrofluid		0.0097	0.0097	0.0048
phase		magnetite	magnetite	magnetite
BET surface area, m^2/g		177.2	159.9	81.7
saturation magnetization of magnetite, emu/g		55	50	60

ments, the possibility of interfacial adsorption of nanoparticles was considered. Surface tensions were therefore measured for water and MEA solutions in the presence of the polymer coated ferrofluid over the volume fraction range of interest, by the Du Nuoy Ring method (Fisher surface tensiomat, model 21). All determinations were repeated twice.

3. Results

3.1. Characterization Studies. A summary of all the characterization studies on the three ferrofluids used in this work is presented in Table 1. Phase characterization of the ferrofluids (using XRD and Raman spectroscopy as reported in our earlier work[15] for the TMAOH coated ferrofluids) revealed the iron oxide phase in the particles to be Fe_3O_4 in all cases, provided care was taken to exclude air during the synthesis procedure. Thus, the particles in the three ferrofluids are all identical with respect to phase composition. Further, VSM results confirmed the superparamagnetic nature of the particles. The saturation magnetization for the particles from the three fluids is shown in Table 1 and may be compared with the literature value of 92 emu/g for pure magnetite.[28,29] A lowering of magnetization is possible due to a disordering of the crystal structure at the surface and due to the complexation of the surfactant with the surface iron atoms.

In selected experiments, X-ray diffraction was also used to examine any effect of the reactions on the particles. Identical XRD patterns were obtained for the particles before and after the experiment, showing that the reactions carried out had no effect on the particles.

Figure 2 shows the particle size distribution of the three types of magnetic nanoparticles used in this work as measured by DLS, and the average diameters are reported in Table 1. While the other characterization studies such as XRD, BET, and microscopy were carried out on the freeze-dried particles, it should be noted that DLS measures the hydrodynamic diameter in suspension, which is *inclusive* of any stabilizing layer (whether of surfactant or polymer) coating the particles. This is the measure that has been used in the sequel in the interpretation of the results.

It was observed that there was no aggregation of nanoparticles after several weeks as evidenced by particle size measurements; further, the size distribution with and without ultrasonication was the same. As Figure 2 shows, the distributions were in general narrow. Crystallite sizes inferred from XRD measurements using the Debye−Scherrer equation[18,30] are also reported in Table 1 and are in good agreement with the other measurements.

Figure 3 shows TEM and HRTEM images of the Fe_3O_4 nanoparticles. The particles are seen to be of spherical shape

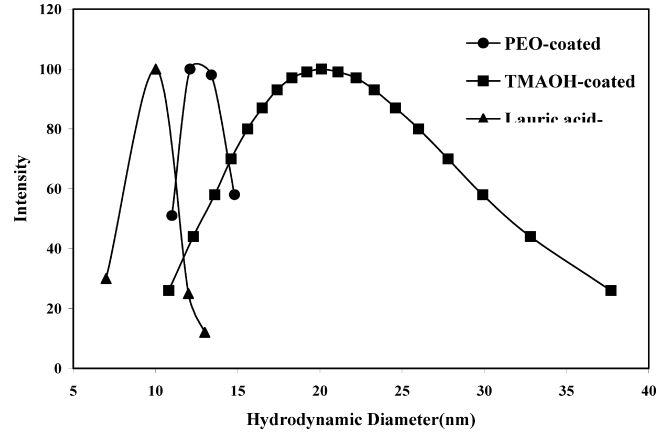

Figure 2. Size distribution of Fe_3O_4 particles used in this work, as measured by DLS.

and in the size range measured by the other techniques. An average size calculated from the analysis of such images is reported in Table 1.

The specific surface area of the particles was measured by BET by the standard single point method. Assuming the particles to be spherical and nonporous, the specific surface area can be related to the average particle size $d_{p,BET}$ by the equation

$$d_{p,BET} = 6000/(\rho S_w) \quad \text{(nm)} \tag{15}$$

where S_w represents the measured specific surface area of the powder in squared meters per gram and ρ is the particle density in grams per cubic centimeter. ρ for magnetite is 5.21 g/cm^3. The good agreement seen in Table 1, between the size thus calculated with the other measures, shows that the particles are nonporous.

It is important that the particle size remains stable during the mass transfer experiments. Komati and Suresh[14] reported that the TMAOH-coated ferrofluid used in their work had the required stability only in tertiary amine solutions (particularly MDEA) and tended to destabilize in primary and secondary amine solutions. Even in MDEA solutions, there was an initial increase in size, which seemed to level off after a certain time. The size variation was not an issue in the WWC since the design of the apparatus ensured that the time for which the particles see the chemical environment is hardly more than the contact time (of the order of 0.1 s). In these experiments, the size of the magnetic nanoparticles in the leaving amine solutions was not much different from the particle sizes in the fluid itself. Komati and Suresh[14] correlated the observed enhancements in the WWC experiments with the particle sizes as measured in the fluid leaving the column. As in that work, the stability of the surfactant coated and polymer coated aqueous ferrofluids were investigated at various concentrations of the several amine solutions used in these studies. Representative results are shown in Figure 4, and it is seen that the polymer coated magnetic nanoparticles are extremely stable in the amine solutions of all concentrations as compared to TMAOH and lauric acid-coated magnetic nanoparticles. The lauric acid-coated ferrofluids were unstable in the amine solutions in general, and somewhat stable in methyldiethanolamine solutions (data for other amines is not shown). Hence, from the point of view of applications in gas−liquid contacting, it is the polymer-coated ferrofluid that is the most suitable. In our studies, for reasons stated above, all the fluids could be used in the WWC, although only the polymer coated ferrofluids could be used in the capillary experiments in which the contact times were longer.

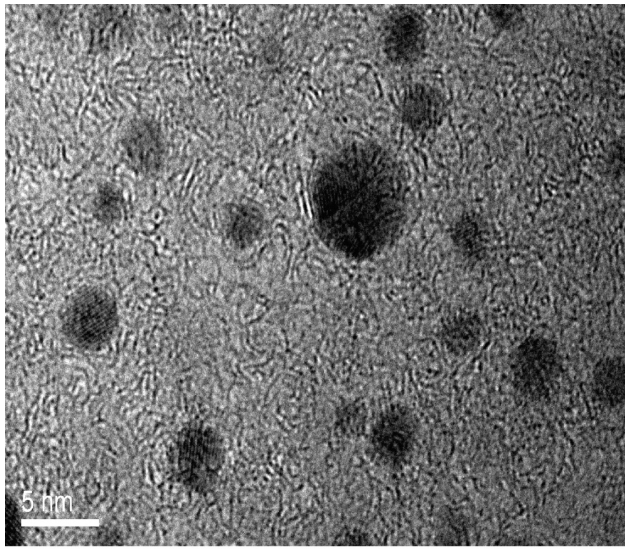

(a)

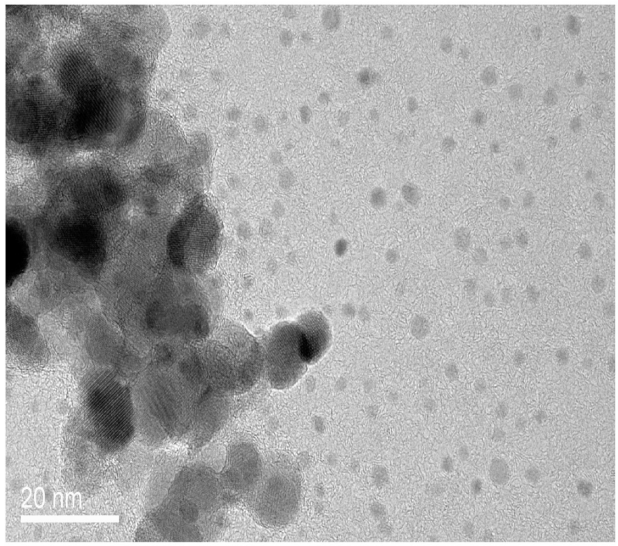

(b)

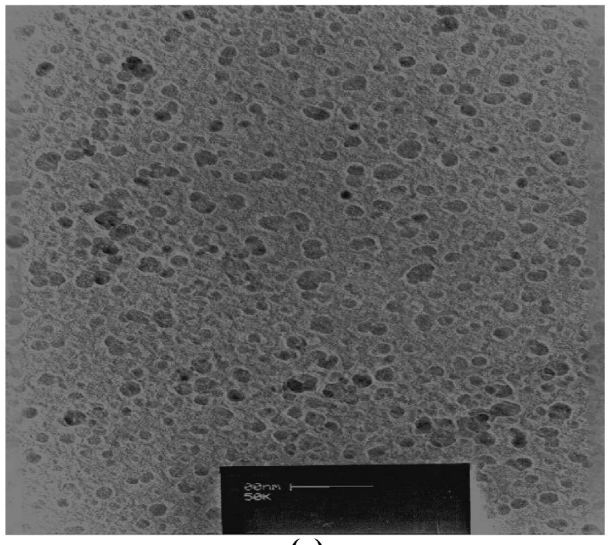

(c)

Figure 3. HRTEM images of (a) TMAOH-coated ferrofluid and (b) lauric acid-coated ferrofluid. (c) TEM image of polymer-coated ferrofluid. The bar in part c represents 100 nm.

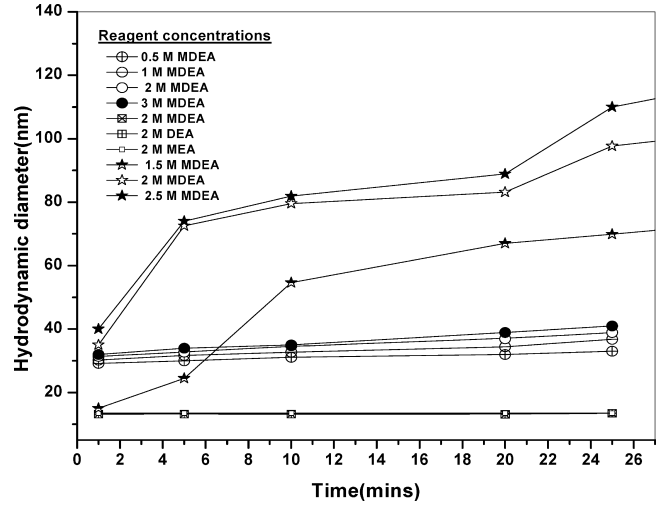

Figure 4. Stability of the three ferrofluids in various amine solutions (MEA monoethanolamine, DEA diethanolamine, MDEA methyl diethanolamine). Square symbols are for polymer-coated ferrofluids, circles are for TMAOH-coated fluids, and stars are for lauric acid-coated fluids.

Since the addition of ferrofluids can, in principle, alter the values of properties important in gas absorption, such as the solubility of the gas in the liquid, solubility determinations were carried out in the presence of ferrofluids as described in the experimental section. TMAOH-coated ferrofluids were used in these studies. The results showed that the solubility was largely insensitive to the presence of the ferrofluid at the concentrations used. If anything, a slight decrease was observed, being of the order of 6% for a volume fraction of solid magnetite of 0.4%.

3.2. Mass Transfer Studies and Enhancements Due to Ferrofluids. 3.2.1. WWC Experiments in the Transition from the Slow to the Fast Regime. Our earlier results[14] with TMAOH-coated ferrofluids in this regime showed that the mass transfer coefficient is enhanced in the presence of the ferrofluid, the extent of enhancement depending on the volume fraction of the solid in the working fluid. Similar results with the other two ferrofluids are shown in the Danckwerts' plots of Figure 5 (a and b). Calculations showed[14] that for a height of the column of 7.6 cm, and concentration of MDEA in the range 1000−1500 mol/m^3, values of the parameters *Ha* and *q* were such that the requirements of slow−fast transition regime could be met. In all calculations on these systems, the values of properties such as the solubility of the gas and diffusivity have been corrected for MDEA solutions as suggested in the literature.[31] Referring to Figure 5 and eq 8, it is seen that the slopes are nearly constant, while the intercepts (which depend on $k_L a$) increase with the volume fraction of the solid in the working fluid. Since visual measurements (lack of ripples) confirm that the area is unaffected by the addition of ferrofluids, these results show that k_L increases as the volume fraction of magnetite is increased.

For O_2 absorption into sodium dithionite solutions, the Danckwerts plot was generated by varying the concentration of the sodium dithionite in the range from 60 to 80 g mol/m^3. The values of *Ha* and *q* are shown in Table 2, and the results (plotted with C_{B0} on the *x*-axis) in Figure 6. For this kinetics, the relation between absorption rate and the mass transfer parameters can be cast as (see eq 8)

$$\left(\frac{R_A a}{C_A^*}\right)^2 = \frac{2k_{mn}D_A a^2}{C_A^*}C_{B0} + (k_L a)^2 \qquad (16)$$

The same feature of a particle-holdup dependent enhancement in k_L, as remarked upon in Figure 6, is seen here also.

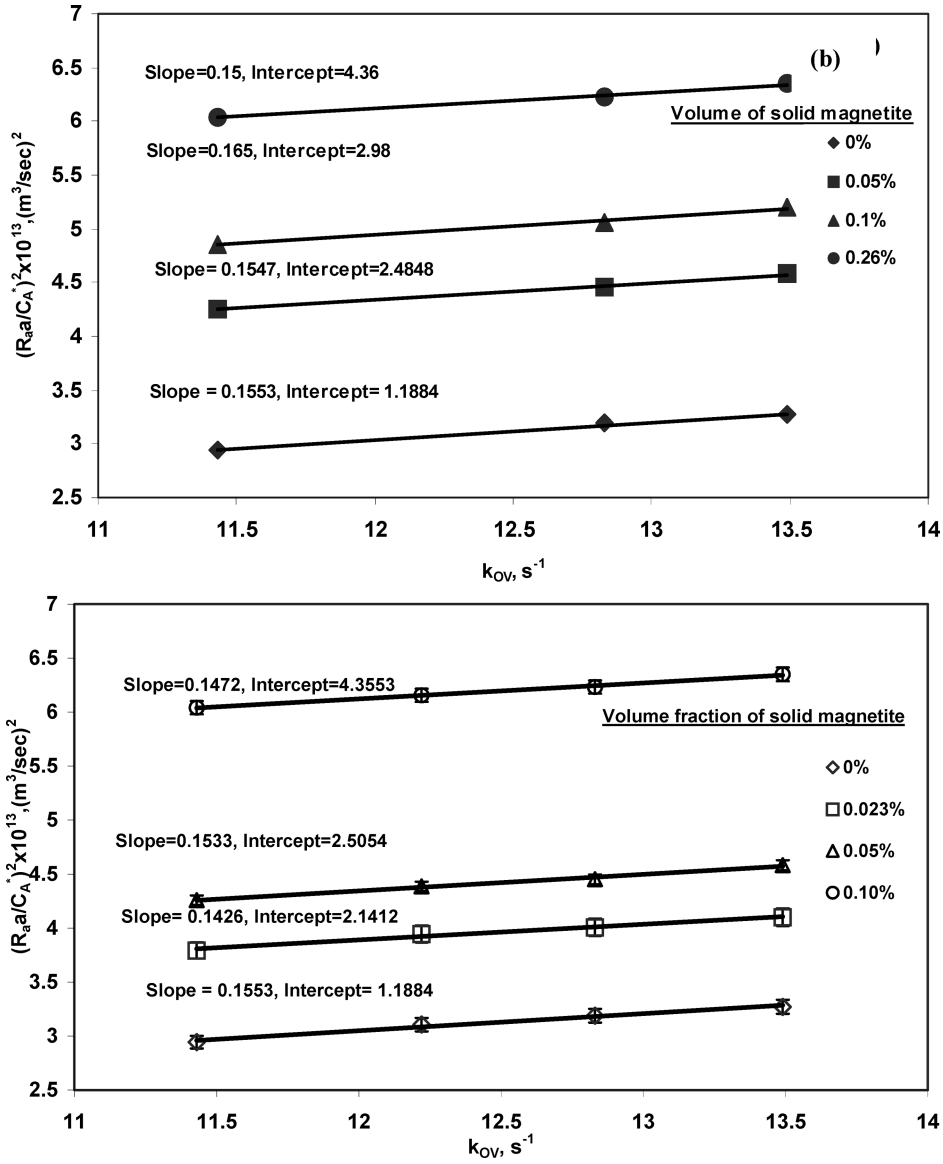

Figure 5. Typical Danckwerts plots of data for absorption of carbon dioxide in methyl diethanolamine solutions with (a) lauric acid-coated ferrofluid and (b) polymer-coated ferrofluid. The particle sizes at the exit of WWC in the two cases were respectively 15 and 13.2 nm as determined by DLS.

Table 2. Values of the Parameters *Ha* and *q* for Slow−Fast Transition Regime Experiments on O_2 Absorption into Sodium Dithionite Solutions in the Wetted Wall Column

length (cm)	$[Na_2S_2O_4]$ (gmol/m^3)	C_A^* (gmol/m^3)	$D_A \times 10^9$ (m^2/s)	$D_B \times 10^9$ (m^2/s)	*Ha*	*q*
17.6	80	1	2.78	1.31	1.15	55
17.6	60	1	2.78	1.31	1.08	44

Mass transfer coefficients obtained as above were treated as first estimates and refined by fitting the data to eq 9 obtained from the penetration theory. Mass transfer coefficient enhancements due to ferrofluid addition have been calculated from such results as

$$E_p = \left(\frac{k_{Lp}}{k_{L0}}\right) \tag{17}$$

where k_{Lp} and k_{L0} are the (physical) mass transfer coefficients determined with and without particles, respectively. Such enhancements have been plotted as a function of the volume fraction of the particles for the three fluids used, in Figure 7. The dependence of the enhancement on the volume fraction of solid magnetite in the ferrofluid can be seen from the figure. The results for the carbon dioxide−MDEA system show that, for the same gas−liquid system, for a given volume fraction, the enhancements in k_L correlate inversely with particle size and are in the order: polymer-coated ferrofluid (13.2 nm) > lauric acid-coated ferrofluids (15 nm) > TMAOH-coated ferrofluids (23 nm). However, for the same particles (polymer coated), the enhancements obtained for the two gas−liquid systems differ, suggesting that the influence of the particle size depends on some other factor not so far considered.

3.2.2. WWC Experiments in the Instantaneous Reaction Regime. Komati et al.[15] found in their studies in the instantaneous reaction regime in a bubble column that, while magnetic nanoparticles enhanced mass transfer coefficients, the enhancements were lower than those observed at the same volume fraction and particle size in the wetted wall column where the regime was one of transition from slow to fast reaction. While they speculated that the smaller depth of penetration in instantaneous reaction was possibly the reason, it remained to be confirmed, especially since the studies were in two different types of equipment.

Instantaneous reaction regime experiments were therefore conducted in the WWC itself in the present study, by employing

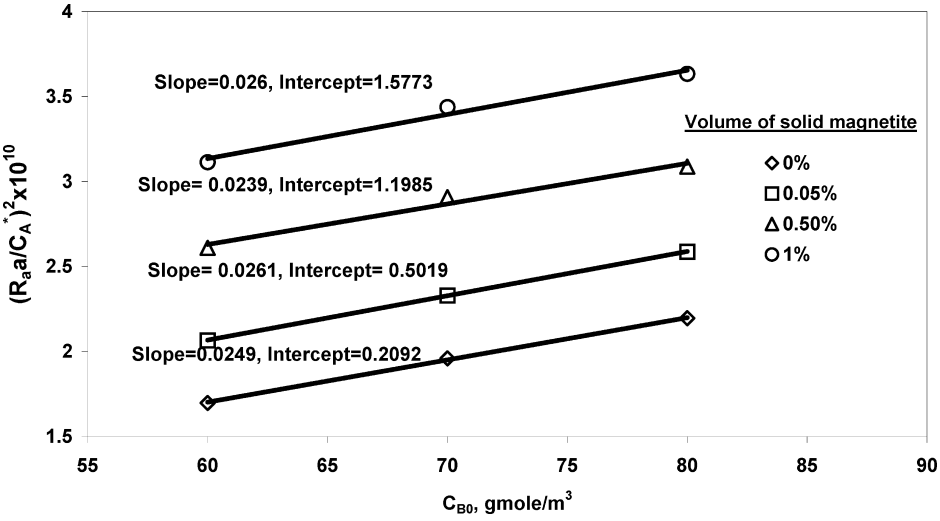

Figure 6. Typical Danckwerts plot of data for absorption of oxygen into sodium dithionite solutions with polymer coated ferrofluids. The size of magnetite nanoparticles at the exit of the column was 13.2 nm as measured by DLS.

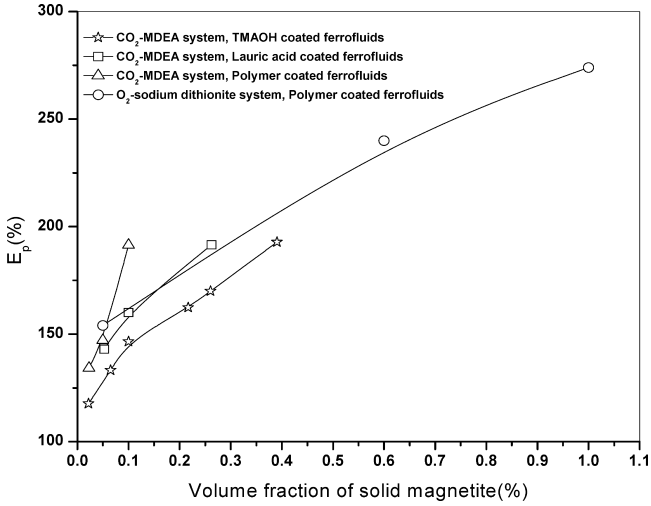

Figure 7. Mass transfer enhancements (%) with different ferrofluids and different gas−liquid systems, plotted as a function of the volumetric holdup used.

the CO_2−MEA system to understand the effect of penetration depth on enhancements. Table 3 shows the values of the parameters employed. From the measured absorption rates, mass transfer coefficients (and their enhancements due to the presence of particles) were calculated as described in the earlier sections.

In the instantaneous reaction regime as remarked earlier, the reaction takes place at a plane, and the penetration of the solute is limited to the region between the gas−liquid interface and this plane. As a first attempt, we could derive a depth of penetration using the precepts of the film theory which, although less correct than the surface-renewal class of theories in a fundamental sense, is known to give results very similar to the latter theories.[21] According to this theory, all concentration variation of a dissolving solute is contained in a "film" of thickness $\delta = D_A/k_L$. Further, the entire film is available for the diffusion of A in all absorption regimes except in the instantaneous reaction regime, in which it is confined to a distance λ, where $\delta/\lambda = E_\infty$. While the film theory would have $E_\infty = (1 + q)$, it has been suggested[23] that a multiplication of this result by the square root of the ratio of diffusivities, viz., $E_\infty = (D_A/D_B)^{1/2}(1 + q)$ (also see eq 12) would give a square-root dependence of the mass transfer coefficient on diffusivity, more in accord with experimental observations.

The above expressions from film theory were accordingly used to plan these experiments, and the position of the reaction plane (and hence the penetration depth) was varied in two ways. In the first set (first three rows of Table 3), the parameters that determine the mass transfer coefficient in the wetted wall column were kept constant and the value of the parameter q was varied through the concentration of MEA. In the second set (last three rows of Table 3), the value of q was kept constant and k_L was varied via the liquid flow rate. Values of δ/λ, calculated as described above, are shown in Table 3. Figure 8 shows the results on mass transfer coefficient enhancements, on the same coordinates as Figure 7. These experiments were conducted with the polymer-coated ferrofluid and, hence, are to be compared with the curve for this fluid in Figure 7. The comparison reveals some interesting features. First, the enhancements are smaller in instantaneous reaction, a result in qualitative agreement with the suggestion of Komati et al.[15] Furthermore, the results show the importance of the penetration depth in addition to the particle holdup and size as parameters—the smaller the value of λ, the smaller the enhancement. These results therefore suggest that it is not the particle size per se, but the particle size in relation to the penetration depth, which is important in determining the enhancing effect of nanoparticles.

3.2.3. WWC Experiments in the Fast Reaction Regime. The results thus far are in regimes where the hydrodynamics influence the rate of absorption. Since the mass transfer coefficient is determined by hydrodynamics as well as molecular diffusivity, it would be interesting to try and separate the role of these two in determining the enhancements due to ferrofluids. The theory of mass transfer with chemical reaction provides an opportunity to do this, since the mass transfer rate in the fast reaction regime is known to be independent of hydrodynamic parameters. The specific rate of absorption in this regime, for a first order reaction, is given by[23]

$$R_A a = C_A^* a\sqrt{D_A k_1} \tag{18}$$

and the mass transfer flux depends only on the product $(D_A k_1)^{1/2}$. The conditions that are needed to be satisfied are $3 < Ha \ll E_\infty$. These conditions could be arranged in our WWC for the CO_2−MDEA system, as Table 4 shows, for a concentration of MDEA of 4000 mol/m^3. A column length of 7.6 cm was employed, and the regime was confirmed by checking for the independence of absorption rate on liquid flow rate (see Table 4). A comparison of absorption rates with and without ferrofluids

Table 3. Values of the Parameters for the Instantaneous Reaction Regime Experiments on CO_2 Absorption into MEA Solutions in the Wetted Wall Column[a]

[MEA] (gmol/m^3)	C_A^*(gmol/m^3)	$D_A \times 10^9$ (m^2/s)	$D_B \times 10^9$ (m^2/s)	$k_L \times 10^4$(m/s)	$\delta \times 10^5$(m)	*Ha*	*q*	δ/λ
60	27.2	2.248	1.875	1.245	1.813	8.1	1.0	2.197
90	27.2	2.248	1.875	1.240	1.813	10.1	1.5	2.737
120	27.0	2.241	1.845	1.239	1.813	11.6	2.0	3.284
220	26.7	2.217	1.802	1.231	1.813	15.7	3.7	5.157
220	26.7	2.217	1.802	1.070	2.110	18.0	3.7	5.157
220	26.7	2.217	1.802	0.950	2.360	19.8	3.7	5.157

[a] The values of δ and δ/λ shown are calculated from the film theory expressions, with eq 12 used for E_∞.

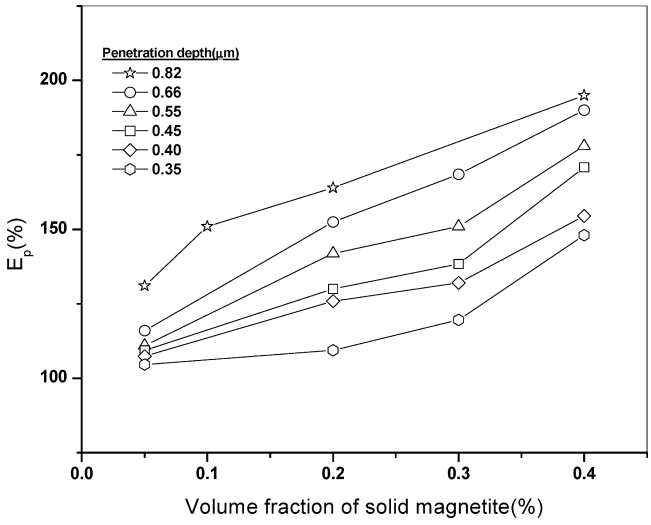

Figure 8. Mass transfer enhancements as a function of the volumetric holdup used, showing the effect of penetration depth. The penetration depths shown in the legend are calculated from Table 3.

Table 4. Experiments in the Fast Reaction Regime with the CO_2−MDEA System for [MDEA] = 4000 gmol/m^{3a}

volume of solid magnetite (%)	flow rate of amine (mL/min)	$k_L \times 10^5$ (m/s)	*Ha*	E_∞	$R_A a$ (mL/min)	percent enhancement $E_p \times 100$
0	180	4.6	3.9	58	20.5	
0	120	4.1	4.4	58	20.6	
0	90	3.7	4.9	58	20.7	
0.05	180	4.6	3.9	58	28.5	138
0.05	120	4.1	4.4	58	28.4	137
0.05	90	3.7	4.9	58	28.4	137
0.3	180	4.6	3.9	58	33.9	164
0.3	120	4.1	4.4	58	34.0	164
0.3	90	3.7	4.9	58	33.9	163

[a] The values of *Ha* and E_∞, as well as the independence of absorption rate on liquid flow rate, confirm the regime. The enhancements shown in the last column are those in absorption rates.

shows an effect of ferrofluids in this case also. One can define a "pseudo" mass transfer coefficient for this case, as the proportionality constant between absorption flux and C_A^*, and calculate an enhancement in this due to ferrofluids. Enhancements so calculated are shown in Table 4. These enhancements will be compared with the earlier presented data on the basis of a scaled particle size in the sequel.

3.2.4. Mass Transfer Studies in the Absence of Flow: Capillary Experiments. The capillary apparatus allows us to probe the particle size-penetration depth effects further. Since mass transfer in this case is purely by an unsteady state diffusion, the penetration depth changes with time, and by making measurements at several values of the contact time, it is possible to realize a range of penetration depths in a single experiment. Second, while WWC experiments involved only reactive systems, this apparatus allows us to study the case of no reaction. Third, it allows us to confirm the hydrodynamics-independent nature of the action of the ferrofluid, which was suggested by the fast regime results, since flow is absent. Finally, we have so far interpreted the experimental results using results deriving from Fickian diffusion uncritically, and the capillary apparatus provides a check on the Fickian nature of the diffusion process. The capillary experiments involve long contact times (comparatively speaking), and so, require a higher degree of stability of the ferrofluid in the working fluid as compared to the WWC. These experiments have therefore been performed with the polymer-coated ferrofluid.

Preliminary experiments were conducted to see if the orientation of the tube had any effect on the results and to ascertain the reproducibility of the experiments. The results were identical irrespective of whether the tube was horizontal or vertical. In repeat experiments, the slug position at the same time was found to be reproducible to within 0.5 mm.

Instantaneous Regime Experiments. These experiments were performed using the absorption of CO_2 into monoethanolamine (MEA) solutions. The concentration of MEA was varied in the range from 90 to 4000 gmol/m^3. It is easily verified that the conditions of instantaneous reaction are satisfied under these conditions, over the entire duration of the experiments, and even after accounting for any enhancement in mass transfer coefficients caused by the presence of particles. At each concentration of MEA, experiments were conducted for several volume fractions of the solid magnetite, in the range from 0.05 to 1%. Figures 9−13 show the results. Each figure plots the variation of slug length vs the square root of time for a constant concentration of MEA, for several ferrofluid holdups. In each case, the base case of absorption into solution without any ferrofluid has been predicted using eq 13 with the literature values of diffusivities, and the comparisons with experimental results are shown.

Experiments at the higher MEA concentrations (especially 4000 mol/m^3) were more difficult than others since the absorption rates were high, and data at these concentrations must be considered less accurate. All things considered, however, the data show a satisfactory linearity on these coordinates, in accordance with eq 13, and hence confirm that the process can be treated as Fickian diffusion with a constant diffusivity. Second, in this case of absorption into a quiescent liquid column as well, a considerable enhancement of the mass transfer rates in the presence of the nanoparticles is clear in all cases, the extent of enhancement increasing as the particle holdup increases. As eq 13 shows, for each experiment, we can calculate an average mass transfer coefficient for each time, and by comparing it with the base case for the same time, an enhancement in accordance with eq 17. Such calculations show the enhancement increasing with time in each case. Since the penetration depth of the solute increases with time (see discussion of eq 10), this is qualitatively consistent with what has been observed in the instantaneous regime studies of the WWC.

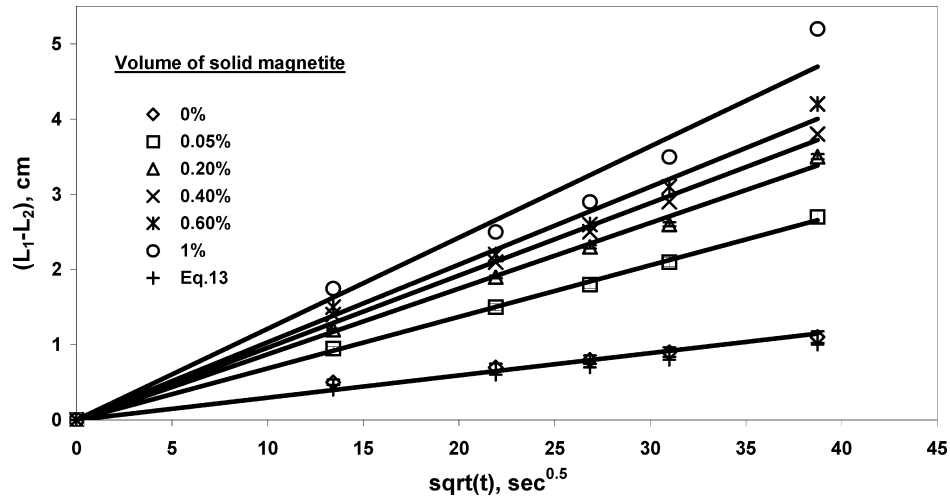

Figure 9. Instantaneous reaction in the capillary: variation of the length of the gas chamber A with time for MEA concentration of 90 g mol/m^3. Note the comparison of experimental data for the base case (no ferrofluid added) with eq 13, for $D_A = 2.24 \times 10^{-9}$ m^2/s, $D_A/D_B = 1.2$.

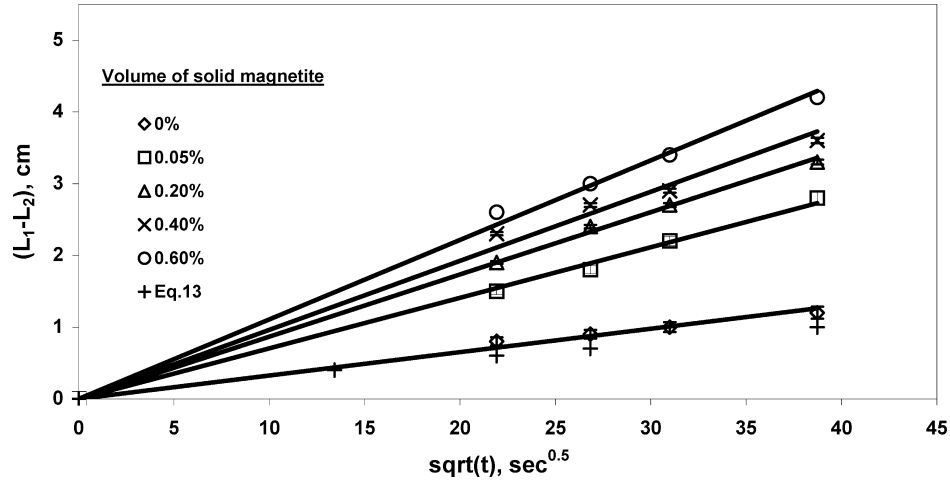

Figure 10. Instantaneous reaction in the capillary: variation of the length of the gas chamber A with time for MEA concentration of 160 gmol/m^3. Note the comparison of experimental data with eq 13, for $D_A = 2.24 \times 10^{-9}$ m^2/s, $D_A/D_B = 1.2$.

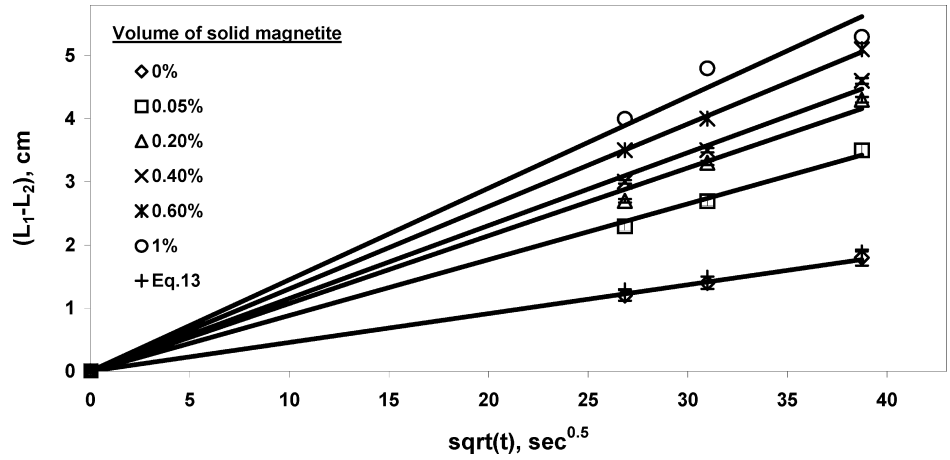

Figure 11. Instantaneous reaction in the capillary: variation of the length of the gas chamber A with time for MEA concentration of 320 gmol/m^3. Note the comparison of experimental data with eq 13, for $D_A = 2.19 \times 10^{-9}$ m^2/s, $D_A/D_B = 1.23$.

Physical Absorption Studies. Since all the above experiments have been conducted with reactive systems, it would be worthwhile ensuring that the rate-enhancing effect of nanoparticles is independent of a chemical reaction being present. The capillary system lends itself ideally to physical absorption studies. These studies were carried out with the CO_2−water system, using the polymer-coated ferrofluid. Interpretation of the data from these experiments is based on eq 7. The data, for several values of particle holdup, are shown in Figure 14. Clearly, both the Fickian (with a constant diffusivity) nature of the diffusion process and an enhancing effect of nanoparticles on the mass transfer coefficient are present even in this case. In

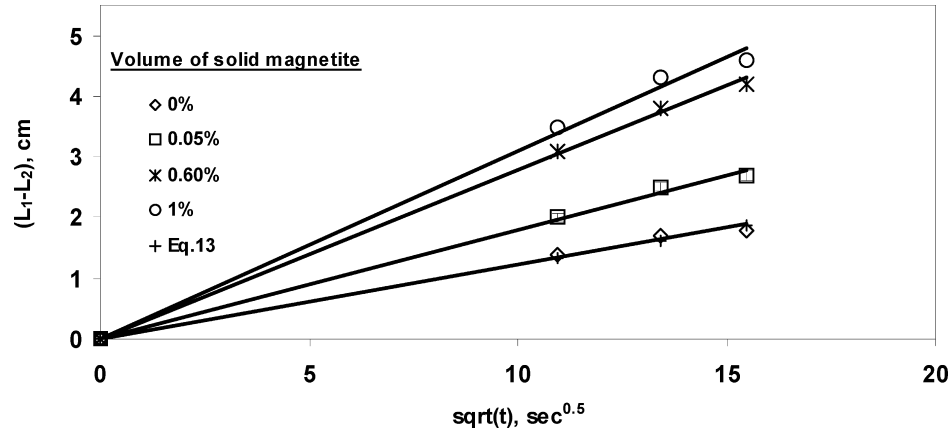

Figure 12. Instantaneous reaction in the capillary: variation of the length of the gas chamber A with time for MEA concentrations of 1000 gmol/m^3. Note the comparison of experimental data with eq 13, for $D_A = 2.019 \times 10^{-9}$ m^2/s, $D_A/D_B = 1.33$.

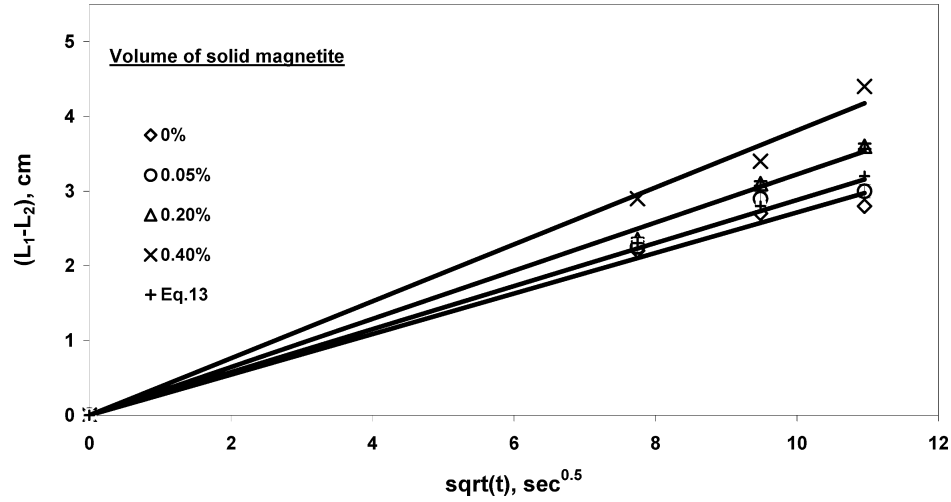

Figure 13. Instantaneous reaction in the capillary: variation of the length of the gas chamber A with time for MEA concentration of 4000 g mol/m^3. Note the comparison of experimental data with eq 13, for $D_A = 1.2403 \times 10^{-9}$ m^2/s, $D_A/D_B = 1.02$.

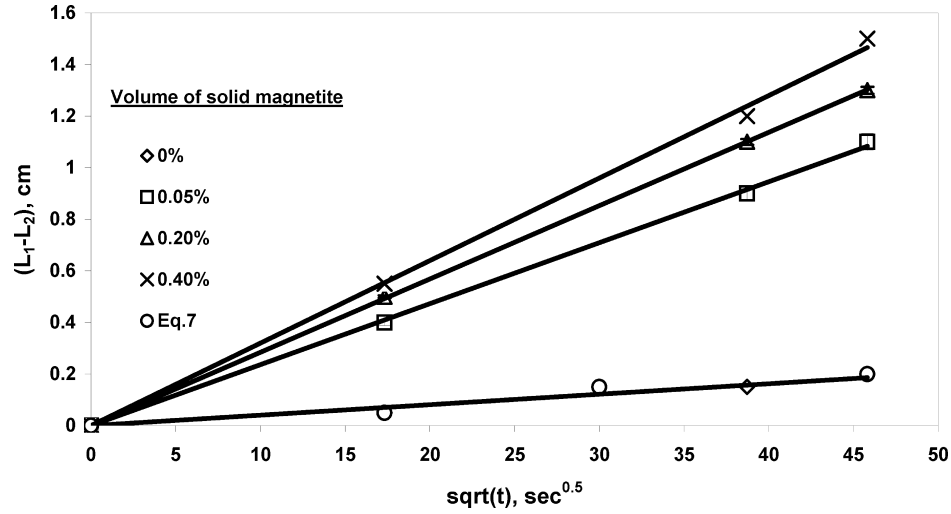

Figure 14. Physical absorption of CO_2 into water in the capillary. Note the comparison for the no ferrofluid case with eq 7, for $D_A = 2.26 \times 10^{-9}$ m^2/s.

the sequel, we shall compare these enhancements with those observed in the earlier experiments.

4. Discussion of the Results

4.1. Analysis of the Results in Terms of Film Theory. The results thus far show that (a) magnetite nanoparticles enhance liquid phase mass transfer coefficients, (b) such enhancement occurs both in the presence as well as in the absence of flow, in the presence and absence of a chemical reaction, and, in the latter case, in all the absorption regimes investigated, and (c) the magnitude of the enhancement depends on the particle size, volumetric holdup, and diffusion length (or penetration depth)

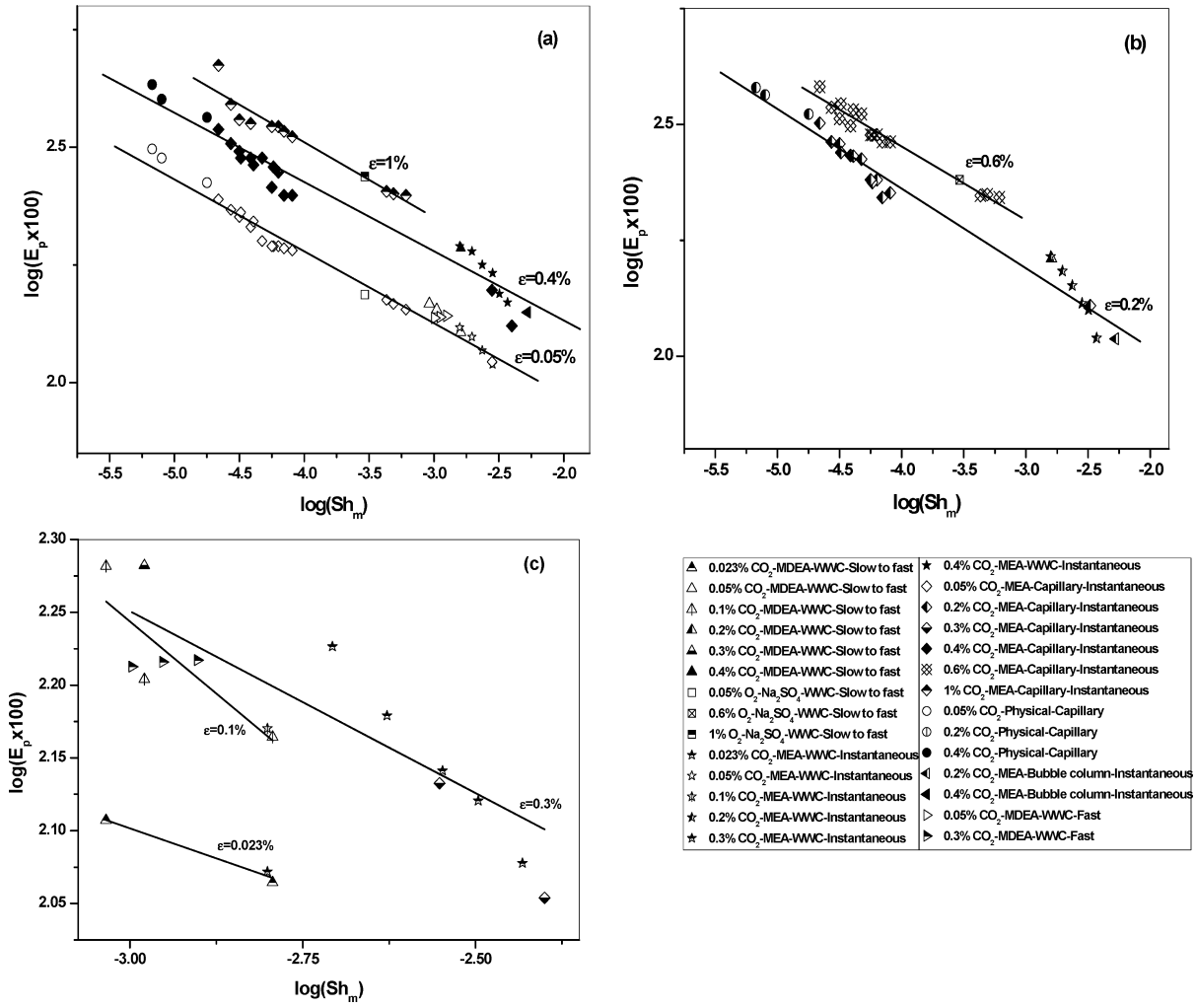

Figure 15. Enhancements due to nanoparticles plotted as a function of the modified Sherwood number (film theory) on log−log coordinates for different values of the particle holdup.

of the solute. In the present section, we shall try to arrive at some general principles that govern this phenomenon and thus unify all the results from these diverse situations.

The results on the particle size−penetration depth effects suggest that a particle size scaled with respect to the penetration depth might be an appropriate parameter in terms of which to seek a correlation of the results. Calculation of a penetration depth according to film theory has been described earlier (section 3.2.2). With these definitions, the scaled particle size referred to above, in absorption regimes where the full thickness of the film is available for the diffusion of A, is nothing but a Sherwood number based on the particle size

$$\frac{d_p}{\delta} = \frac{k_L d_p}{D_A} = Sh_p \tag{19}$$

For the case of the instantaneous reaction regime, correcting for the restriction of the field of diffusion, the scaled particle size becomes

$$\frac{d_p}{\lambda} = \frac{k_L d_p}{D_A}\left(\frac{\delta}{\lambda}\right) = Sh_p E_\infty \tag{20}$$

We may therefore plot the enhancements E_p observed, as a function of a modified Sherwood number Sh_m, which is given by eq 20 for instantaneous reactions and eq 19 for all other cases. Figure 15 (a−c) shows such plots for different values of the particle holdup. In addition to the results of this work presented in the previous sections, the bubble column data of Komati et al. (2007) are also plotted here. In the experiments of Komati et al.,[15] carbon dioxide was absorbed into methyldiethanol amine (MDEA) solutions for a known time in the bubble column, and the mass transfer coefficient was determined by integrating the rate expression for the instantaneous regime. Enhancements due to ferrofluids have been calculated from that data in the usual manner by comparing the coefficients obtained in these cases with those for the base case.

In Figure 15, the data for different particle holdups are plotted in different panels for clarity, and the data for some holdups, for which only a limited range of Sh_m was covered, are plotted separately in Figure 15c.

The data generally follow a straight line, with a slightly larger scatter at lower enhancements. It should be noted that the small enhancement data carry greater error due to the difficulties in determining small increases in the rates of absorption over the base case (the data in Figure 15c are entirely in this range). In general however, a good correlation is seen in Figure 15 showing that Sh_m, as a correlating parameter, brings together results for a given particle holdup, across all regimes, two gas−liquid systems, three types of particles, and three contacting devices. Enhancements observed in the attempts made to reproduce the same value of Sh_m in different contacting situations and regimes are particularly noteworthy. For example, a value of $Sh_m = 0.0028$ (log $Sh_m = -2.55$) was obtained in instantaneous

reaction regime in capillary tube as well as in the WWC; a value of about 0.00159 (log $Sh_m = -2.7986$) was obtained in the slow−fast transition regime and instantaneous regime experiments for WWC, and nearly equal values of 0.0037 (log $Sh_m = -2.43$) and 0.004 (log $Sh_m = -2.39$) were obtained in WWC and capillary (instantaneous regime), all at several values of the particle volume holdup. As Figure 15 shows, the enhancements obtained in these cases were clearly independent of the other parameters, for a given value of the particle holdup and Sh_m. Further, enhancements in the bubble column correlate well with other data at the same holdup, and those in the fast reaction regime are similar to other regimes at similar values of Sh_m. (0.001252−0.001007) (log $Sh_m = -2.9024$ to -2.996).

The best fit lines shown in Figure 15a and b have nearly the same slope; the slopes averaging out to 0.1572. The intercepts depend on the holdup. In order to give a greater weightage to the data at higher enhancements (which data are more numerous), the slopes of all lines were fixed at the average value and the intercepts estimated by regression. These intercepts, when plotted against log (holdup) once again gave a straight line. By this procedure, the following correlation for the enhancement due to nanoparticles in terms of the holdup ε and modified Sherwood number was finally obtained:

$$E_p = 1.621\varepsilon^{0.171} Sh_m^{-0.157} \tag{21}$$

4.2. Analysis of the Results in Terms of the Theory of Unsteady State Absorption. While film theory has been used in the above analysis on the grounds that it is simpler and known to give similar results to the more sophisticated unsteady state theories, it may be argued that the film theory is not appropriate in this case, the situation being one of unsteady state absorption in all cases except in the bubble column, where any theory (film, penetration, or surface renewal) is only an approximation. In unsteady state diffusion, a finite depth of penetration of A can be calculated only for the case of Instantaneous reaction, where it is determined by the location of the reaction plane as given by $2\beta\sqrt{t}$, with β being given by eq 11. Since our enhancements are based on measurements of average rates of absorption over a time period, we would attempt to correlate these with the average penetration depth, obtained by averaging the (instantaneous) penetration depth as

$$\bar{\lambda} = \frac{1}{t}\int_0^t 2\beta\sqrt{t'\,\mathrm{d}t'}$$

t' being a dummy integration variable. Substitution of this into the expression $(d_p/\bar{\lambda})$ gives

$$(d_p/\bar{\lambda}) = \left(\frac{3\sqrt{\pi}}{8}\right)\left(\frac{Sh_p}{\beta/\sqrt{D_A}}\right) \tag{22}$$

For small values of $(\beta/\sqrt{D_A})$, eq 10 shows that the last term is brackets is (ShE_∞), thus giving a formulation that agrees with the film theory formulation.

In other regimes, concentration profiles extend to infinity, and therefore, penetration depths need to be *defined*, say as the distance from the interface which contains a *specified percentage* of the variation in the concentration of A. In physical absorption, this penetration depth is given by $n(D_A t)^{1/2}$, where the value of n depends on the percentage of concentration variation one wants contained in the penetration depth; 53% of the variation occurs in $(D_A t)^{1/2}$, 85% in $2(D_A t)^{1/2}$, 97% in $3(D_A t)^{1/2}$, etc. The *average* penetration depth is obtained as before, and substitution into the expression $(d_p/\bar{\lambda})$ gives

$$(d_p/\bar{\lambda}) = \left(\frac{3\sqrt{\pi}}{4n}\right)(Sh_p) \tag{23}$$

The scaled particle diameter is thus proportional to the particle Sherwood number in this case, with the proportionality constant depending on the value of n chosen.

When a chemical reaction accompanies diffusion, we obtain a penetration depth from the following consideration. The chemical enhancement factor E (for which the unsteady state theory gives expressions in different regimes) is the ratio of the average concentration gradient at the interface in the presence of chemical reaction to that without. The penetration depths may be assumed to vary inversely as the gradient at the interface for the same concentration driving force. We may therefore obtain penetration depths in the different enhancement regimes (slow to fast transition and fast reaction) by dividing $\bar{\lambda}$ for the case of physical absorption by E. These considerations show that, for these regimes

$$(d_p/\bar{\lambda}) = \left(\frac{3\sqrt{\pi}}{4n}\right)(Sh_p E) \tag{24}$$

Thus, with the unsteady state theory, we are led to a definition of a modified Sherwood number Sh'_m (to which the scaled particle size is proportional), which consistently incorporates the chemical enhancement factor in *all* regimes, not just for the case of instantaneous reaction.

It remains to fix a value of n in order to compare the correlation between E_p and Sh'_m for the data in instantaneous reaction with other regimes on a uniform basis. We do this by looking for that value of n (among small integers 1, 2, 3), which leads to the best correlation of all the data. For the present data, the above procedure gave $n = 3$.

Figure 16 shows a log−log plot of the enhancement due to nanoparticles, plotted as a function of ($Sh'_m = ShE$). On processing the intercepts of the constant holdup lines as before, the correlation suggested in this case is

$$E_p = 1.519\varepsilon^{0.169} Sh'^{-0.159}_m \tag{25}$$

It is interesting that this correlation is only marginally different from the one obtained from film theory considerations. In Figure 17, we compare the experimental data with eq 25 (comparison with eq 21 is not shown since the unsteady state theory is the better one to use for our experiments). It is seen that the correlation is able to bring together all the data irrespective of the apparatus, presence or absence of a reaction, absorption regime, and the gas−liquid system. Also included in Figure 17 are some data from Olle et al.[13] for physical absorption in a stirred beaker in the presence of magnetic nanoparticles, processed in a manner similar to our data. It is clear that the data of Olle et al.[13] are also well-correlated by eq 25. The other data from Olle et al.,[13] which are for chemical absorption, could not be compared with the correlation because the authors have reported enhancements in $k_L a$ which cannot be separated into those in k_L and a.

4.3. Some Outstanding Issues. While the correlations above are certainly useful from the point of view of predicting enhancements for any situation, and therefore for an exploitation of the rate intensification effect of nanoparticles, the mechanism by which this intensification is brought about remains unclear. The theories for the enhancement of mass transfer rates by particles finer than diffusion film thickness[9−11] were tested in this context but would require unreasonably high values of the partition coefficient of the solute between the particulate phase and the liquid phase (of the order of 10^3) to predict the kind of enhancements observed. Recently Nagy et al.[32] have attempted to model mass transfer enhancement by nanofluids and come to a similar conclusion. The results of these authors show that

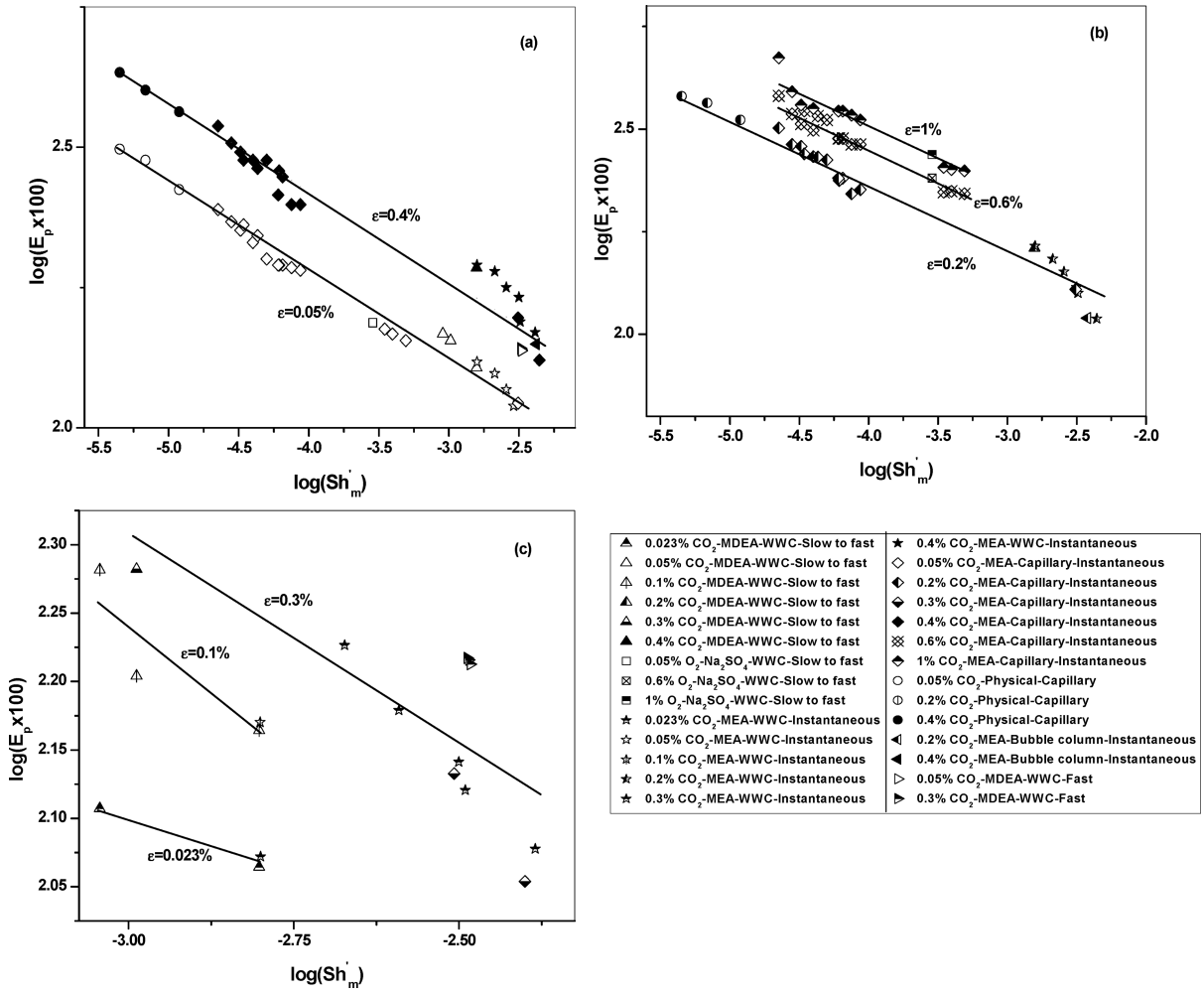

Figure 16. Enhancements due to nanoparticles plotted as a function of the modified Sherwood number (penetration theory) on log−log coordinates for different values of the particle holdup.

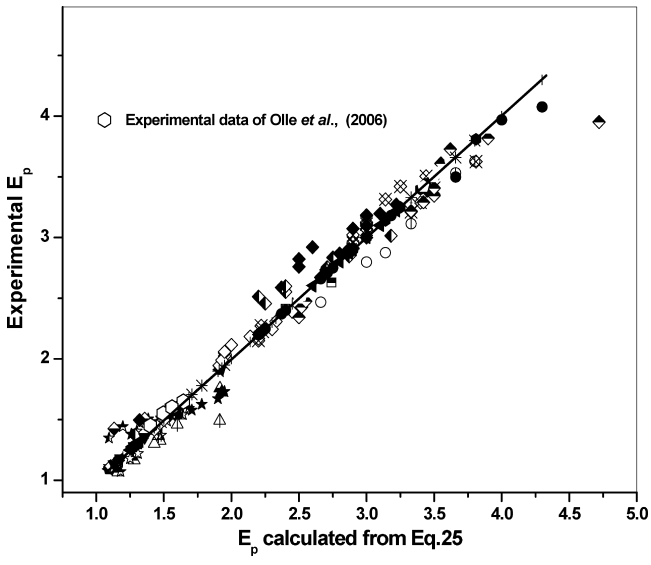

Figure 17. Parity plot comparing experimental data with eq 25. For meanings of symbols, refer to the key in Figures 15 and 16. The data of Olle et al.[13] for Fe_3O_4 nanoparticles ($d_p = 25$ nm, $Re = 0.08$, $Sc = 216$, $Sh_m = 1.851 \times 10^{-4}$) are also shown here for comparison.

an increased diffusivity has to be assumed in any mass transfer model (they used a heterogeneous model to account for particle effects) in order to fit the rate data in the presence of nanoparticles. They invoked a convective motion of the continuous liquid phase induced by the Brownian motion of the nanoparticles to explain the enhanced diffusivity. The small values of the modified Sherwood number at which enhancements are seen in our experiments do suggest that each nanoparticle has an "effective size", or a "zone of influence", much larger than itself, which can be understood as the volume of the continuous phase that is perturbed by its motion.

It would be interesting, in the light of the above discussion, to estimate diffusivities from our data and examine the enhancements in the presence of nanoparticles. After all, our experiments have shown that the presence or absence of flow makes no difference to the enhancement obtained. If the increase observed in k_L were actually a manifestation of the increased diffusivities in the presence of nanoparticles, we would expect the ratio ($k_L/\sqrt{D_A}$) to remain constant. This ratio is approximately determined from the slope and intercept of the Danckwerts' plots (Figure 5 and 6). It is interesting to note that the ratio does not remain constant, but increases with particle holdup. Initial efforts[14] to determine diffusivity of the gas through liquid films in the presence and absence of nanoparticles showed no effect, but calculations in the light of the preceding insights show that the modified Sherwood numbers for these experiments would be so large that no enhancement would be expected in any case. Attempts to make thicker films in such experiments and thereby reduce the value of Sh_m were not successful. We therefore estimated the diffusivities in all the model apparatuses (wetted wall, capillary) from which data on absorption rates were

Table 5. Percentage Enhancement in Diffusivity

volume fraction of solid magnetite, %	capillary		WWC		
	instant	physical	instant	slow to fast	fast
0.023				124	
0.05	934	953	203	139	190
0.1				217	
0.2	2060	1360	391		
0.3					282
0.4	3040	1724	678		
0.6	3550				
1	4840				

available, since the contact time in these apparatuses is well-defined. Nonlinear regression tools from MATLAB were used to fit the data to the appropriate expressions available from the theory of unsteady state absorption, with and without reaction.[21] Enhancements in diffusivity due to nanoparticle addition were calculated from these results as

$$\text{percent enhancement} = 100E_{D,p} = \left(\frac{D_{A,\text{ferrofluid}}}{D_{A,\text{noferrofluid}}}\right)100 \tag{26}$$

These enhancements are reported in Table 5. Because of the square-root relationship between absorption flux and diffusivity, errors in the measurement of the former get magnified when we attempt to estimate the latter. Even accounting for this however, Table 5 does not show as neat a correlation as the results for mass transfer coefficients. In general, it is observed that cases where the concentration profile of the gas is steep and located close to the interface exhibit a greater enhancement in diffusivity than those in which the concentration profile extends deeper into the liquid phase. Further, the longer contact time data (capillary) generally show higher enhancements than the shorter contact time data. The possibility of interfacial adsorption of the particles was therefore considered. It is possible that the time scale of such an adsorption process is small enough that equilibrium is achieved in the long contact time experiments, but not in the short contact time experiments. Surface tension measurements were therefore carried out, and did show a lowering in the presence of particles, suggesting interfacial adsorption. Attempts to correlate capillary data with the "interfacial" holdup, and the WWC data, with the "bulk" holdup, were, however, not entirely successful in bringing together all the data. We now believe that diffusivity measurements in homogeneous media in the presence and absence of nanoparticles, and molecular dynamics simulations to understand and interpret the results, are the next steps necessary in explaining the anomalous transport properties of nanofluids. Such studies are currently in progress.

Conclusions

The effect of magnetic iron oxide nanoparticles on the enhancement of gas−liquid mass transfer rate has been studied in this work, in different contactors, and employing different reactions and different absorption regimes. The results conclusively establish the fact of enhancement in mass transfer coefficients, and rule out any other cause (such as changes in interfacial area or solubility, adsorptive, or catalytic effects) behind the observations. The volumetric holdup of the nanoparticles, and their size in relation to the depth of penetration of the diffusing solute emerge as the key parameters that determine the mass transfer enhancements. Correlations have been proposed in terms of a modified Sherwood number and particle volumetric holdup, which enable a prediction of mass transfer enhancements in such situations. It appears that there is a fundamental enhancement of the molecular diffusivity due to the presence of nanoparticles, the exact mechanism of which remains unclear at present. However, assuming a "zone of convective disturbance" around each particle helps rationalize the small values of the modified Sherwood number at which enhancements are observed.

Acknowledgment

One of the authors (S.K.) was supported at different stages of the work by grants from the Ministry of Human Resource Development (MHRD), Govt. of India, and Newreka Green-Synth Ltd., Mumbai.

Notation

a = interfacial area, m^2
C_A^* = solubility of the gas A in the liquid, $gmol/m^3$
C_{B0} = concentration of B in the liquid phase, $gmol/m^3$
C_G = concentration of gas in chamber A, $gmol/m^3$
d_p = particle diameter, nm
D_A = diffusivity of A in the liquid phase (m^2/s)
D_B = diffusivity of B in the liquid phase (m^2/s)
E = chemical enhancement factor
$E_{D,p}$ = enhancement in diffusivity due to nanoparticles defined in eq 26
E_p = enhancement in k_L defined in eq 17
H = Henry's law coefficient, atm/gmol
Ha = Hatta number, dimensionless parameter defined in eq 2
k_1 = first-order rate constant, 1/s
k_{Li} = instantaneous physical mass transfer coefficient, m/s
k_{L0} = liquid side physical mass transfer coefficient in the absence of particles, m/s
k_{Lp} = liquid side physical mass transfer coefficient in the presence of particles, m/s
k_{mn} = reaction rate constant for the (m, n)th order gas−liquid reaction
L = instantaneous length of the gas slug in capillary, m
L_1 = initial length of the gas slug in capillary experiments, m
L_2 = final length of the gas slug at time t in capillary experiments, m
m = reaction order with respect to gas phase A
n = reaction order with respect to liquid phase B
q = dimensionless parameter defined in eq 3
R_A = absorption flux, $mol/(m^2\ s)$
R_{Ai} = instantaneous value of the absorption flux, $gmol/(m^2\ s)$
Sh'_m = modified Sherwood number defined in eq 25 for unsteady state theory calculations
Sh_m = modified Sherwood number defined in eq 21 for film theory
Sh_p = Sherwood number based on particle size defined in eq 19 for film theory
S_w = specific surface area of the powder, m^2/kg
t = time, s
z = stiochiometric coefficient

Greek

β = parameter defined in eq 11
δ = film thickness according to film theory, μm
ε = volume of solid magnetite, %
λ = penetration depth according to film theory, μm
$\bar{\lambda}$ = average penetration depth defined according to penetration theory
ρ = density of solid magnetite, kg/m^3

Literature Cited

(1) Gandhi, S. K. Thermal properties of nanofluids: Controversy in making. *Curr. Sci.* **2007**, *92*, 717–718.

(2) Masuda, H.; Ebata, A.; Teramae, K.; Hishinuma, N. Alternation of thermal conductivity and viscosity of liquid by dispersing ultra-fine particles. *Netsu Bussei (Japan).* **1993**, *4*, 227–233.

(3) Lee, S.; Choi, S.; Eastman, J. Measuring thermal conductivity of fluids containing oxide particles. *J. Heat Transfer−Trans. Asme.* **1999**, *121*, 280–289.

(4) Wen, D.; Ding, Y. Experimental investigation into convective heat transfer of nanofluids at the entranced region under laminar flow conditions. *Int. J. Heat Mass Transfer* **2004**, 5181.

(5) Das, S.; Putra, N.; Thiesen, P.; Roetzel, W. Temperature dependance of thermal conductivity enhancement for nanofluids. *J. Heat Transfer−Trans. Asme.* **2003**, *125*, 567.

(6) Vassallo, P.; Kumar, R.; Damico, S. Pool boiling heat transfer experiments in silica-water nanofluids. *Int. J. Heat Mass Transfer* **2004**, *47*, 407.

(7) Bang, I.; Chang, S. Boiling heat transfer performance and phenomena of Al_2O_3−water nanofluids from a plain surface in a pool. *Int. J. Heat Mass Transfer* **2005**, *48*, 2407–2419.

(8) Yang, Y.; Zhang, Z.; Grulke, E.; Anderson, W.; Wu, G. Heat transfer properties of nanoparticle-in-fluid dispersions (nanofluids) in laminar flow. *Int. J. Heat Mass Transfer* **2005**, *48*, 1107–1116.

(9) Mehra, A. Intensification of multiphase reactions throug the use of microphase. 1. Theoretical. *Chem. Eng. Sci.* **1988**, *43*, 899.

(10) Mehra, A.; Pandit, A.; Sharma, M. Intensification of multiphase reactions throug the use of microphase.2. Experimental. *Chem. Eng. Sci.* **1988**, *43*, 913.

(11) Bruining, W.; Joosten, G.; Beenackers, A.; Hofman, H. Enhancement of gas-liquid mass transfer by a dispersed 2nd liquid phase. *Chem. Eng. Sci.* **1986**, *41*, 1873.

(12) Suresh, A. K.; Bhalerao, S. Rate intensification of mass transfer process using ferrofluids. *Ind. J. Pure Appl. Phys.* **2001**, *40*, 172–184.

(13) Olle, B.; Bucak, S.; Tracy, C. H.; Bromberg, L.; Alan Hatton, T. Enhancement of oxygen mass transfer using functionalized magnetic nanoparticles. *Ind. Eng. Chem. Res.* **2006**, *45*, 4355.

(14) Komati, S.; Suresh, A. K. CO_2 absorption into amine solutions: a novel strategy for intensification based on the addition of ferrofluids. *J. Chem. Tech. Biotech.* **2008**, *83*, 1094.

(15) Komati, S.; Rajagopal, M.; Suresh, A. K. Synthesis, characterization and testing for ferrofluids for mass transfer intensification. *Int. J. Chem. Sci.* **2007**, *5*, 1913–1928.

(16) Krishnamurthy, S.; Bhattacharya, P.; Phelan, P. E. Enhanced mass transport in nanofluids. *Nano Lett.* **2006**, *6*, 419–423.

(17) Kim, J. K.; Jung, J. Y.; Kang, Y. T. The effect of nano-particles on the bubble absorption performance in a binary nanofluid. *Int. J. Refrigeration* **2006**, *29*, 22.

(18) Massart, R. Preparation of aqueous magnetic liquids in alkaline and acidic media. *IEEE Trans. Magn.* **1981**, *17*, 1247.

(19) Moeser, G. D.; Roach, K. A.; Greeen, W. H.; Hatton, T. A.; Laibinis, P. E. High gradient magnetic separation of coated magnetic nanoparticles. *AIChE. J.* **2004**, *50*, 2835.

(20) Roberts, D.; Danckwerts, P. V. Kinetics of CO_2 absorption in alkaline solutions. *Chem. Eng. Sci.* **1962**, *17*, 961–969.

(21) Danckwerts, P. V. *Gas liquid reactions*; McGraw Hill Company: New York, 1970.

(22) Jhaveri, A. S.; Sharma, M. M. Absorption of oxygen in aqueous alkaline solutions of sodium dithionite. *Chem. Eng. Sci.* **1968**, *23*, 1–8.

(23) Doraiswamy, L. K.; Sharma, M. M. *Heterogeneous Reactions; Analysis, Examples and Reactor Design*; Wiley: New York, 1984.

(24) Laddha, S. S.; Dackwerts, P. V. Reaction of CO_2 with ethanolamines: kinetics from gas-absorption. *Chem. Eng. Sci.* **1981**, *36*, 3–479.

(25) Hikita, H.; Asai, S.; Ishikawa, H.; Honda, M. The kinetics of reactions of carbon dioxide with monoethanolamine, diethanolamine and triethanolamine by a rapid mixing method. *Chem. Eng. Sci.* **1977**, *13*, 7.

(26) Al-Ghawas, H. A.; Hagewiesche, D. P.; Ruiz-Ibanez, G.; Sandall, O. C. Physicochemical properties important for carbon dioxide absorption in aqueous methyldiethanolamine. *J. Chem. Eng. Data* **1989**, *34*, 385–391.

(27) Haimour, N. M. Solubility of N_2O in Aqueous Solutions of Diethanolamine at Different Temperatures. *J. Chem. Eng. Data* **1990**, *35*, 177–178.

(28) Cornell, R. M.; Schwartzman, U. *Iron oxides: structure, properties, reactions, occurrence and uses*, 2nd revised ed.; Weinheim Wiley-VCH GmbH: New York, 2003.

(29) Shimoiizaka, J. N. K.; Fujita, T.; Kounosu, A. Sink-float separators using permanent magnets and water based magnetic fluid. *IEEE Trans. Magn.* **1980**, *16*, 368–371.

(30) Taylor. A. *X-Ray Metallography*; Wiley: New York, 1961; p 674.

(31) Ko, J.; Li, M. H. Kinetics of absorption of carbon dioxide into solutions of N-methylsiethanolamine + water. *Chem. Eng. Sci.* **2000**, *55*, 4139–4147.

(32) Nagy, E.; Feckzco, T.; Koroknai, B. Enhancement of oxygen mass transfer in the presence of nanosized particles. *Chem. Eng. Sci.* **2007**, *62*, 7391–7398.

Received for review February 23, 2009
Revised manuscript received September 20, 2009
Accepted October 30, 2009

IE900302Z